ChemComm

COMMUNICATION

View Article Online
View Journal | View Issue

Cite this: *Chem. Commun.*, 2024, **60**, 6003

Received 13th March 2024,
Accepted 10th May 2024

DOI: 10.1039/d4cc01176g

rsc.li/chemcomm

Evaluating the native oxide of titanium as an electrocatalyst for oxalic acid reduction†

Halilu Sale,[ab] Zeliha Ertekin,[ac] Paula L. Lalaguna,[a] Malcolm Kadodwala [a] and Mark D. Symes *[a]

Herein, we show that unmodified titanium electrodes bearing the naturally-forming native Ti_xO_y coating display superior activity for the electroreduction of oxalic acid to glyoxylic acid and glycolic acid compared to Ti-based electrodes that have been deliberately modified for this purpose, in terms of both oxalic acid conversion and overall yields of reduced products.

Oxalic acid holds considerable promise as a sustainable chemical feedstock because it can be directly synthesised from carbon dioxide gas with high selectivity through electrochemical or catalytic methods.[1,2] Oxalic acid is used in various industrial processes as a precursor to other chemicals, including glyoxylic and glycolic acids. During the electrochemical reduction of oxalic acid, Amin *et al.*[3] reported that oxalic acid is first reduced by two electrons to give glyoxylic acid. Glycolic acid can then be produced by further reduction in a sequence of concerted two-proton, two-electron transfers (Fig. 1).[4]

The electrochemical reduction of oxalic acid is important for sustainable chemical synthesis, as it transforms oxalic acid into valuable products like glyoxylic acid and glycolic acid without the need for fossil fuel-derived substrates.[4–6]

Glyoxylic acid and glycolic acid are added-value chemicals predicted to have a combined global market of over one billion US dollars by 2025.[7,8] Glyoxylic acid is widely used as an intermediary component in the production of various chemicals, including pharmaceuticals, dyes, plastics, cosmetics and assorted food and personal care products.[9,10] Glycolic acid has multiple uses as an α-hydroxy acid: it is used as a whitening and tanning agent in textiles, a flavouring agent in food, and a biodegradable monomer in thermoplastic polymers like polyglycolic acid (PGA), which is often used in therapeutic devices.[8,11] Therefore, electrolytic oxalic acid reduction is of considerable importance for net-zero chemical synthesis, but finding the right electrode material and catalyst for an efficient reaction remains challenging.

Materials like lead, graphite and dimensionally stable cathodes have limitations, including deactivation, low current efficiency, poor selectivity for the products of interest, and insufficient conductivity.[12,13] Therefore, there is a need to explore alternative materials for efficient electroreduction of oxalic acid to glyoxylic acid and glycolic acid. To this end, titanium is considered a promising material for oxalic acid reduction due to its durability, low cost, and non-toxicity. Its thin yet robust oxide coating protects the underlying metal whilst maintaining high electrode conductivity. This partially amorphous titanium oxide protective layer possesses self-healing properties, rapidly re-forming in the event of damage, as reported by Wang *et al.*[14] This protective layer, consisting of various titanium species (Ti(II), Ti(III), and Ti(IV)), has oxygen vacancies, and is herein referred to as Ti_xO_y. Through loss of oxygen atoms from their crystalline lattice, titanium suboxides demonstrate exceptional electrical conductivity and notable visible light absorption properties, displaying diverse colours. These inherent properties facilitate ion and charge transport, making titanium suboxides well-suited for various applications in electrocatalysis.[15–18] The chemical inertness thus afforded to titanium electrodes allows them to perform electrochemical processes in harsh environments without degradation.

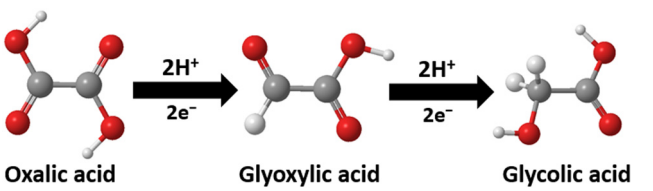

Fig. 1 A pathway showing the reduction of oxalic acid to glyoxylic acid and glycolic acid. Colour code: white = hydrogen, red = oxygen, grey = carbon.

[a] *School of Chemistry, University of Glasgow, G12 8QQ Glasgow, UK. E-mail: mark.symes@glasgow.ac.uk*
[b] *Energy Commission of Nigeria, Plot 701c, Garki-Abuja, Nigeria*
[c] *Hacettepe University, Faculty of Science, Department of Chemistry, Beytepe, 06800 Ankara, Turkey*

† Electronic supplementary information (ESI) available. See DOI: https://doi.org/10.1039/d4cc01176g

Table 1 Average faradaic efficiency, oxalic acid conversion, percentage yields and current densities for the electrochemical reduction of oxalic acid on titanium electrodes for 2 hours at 25 °C

Entry	Applied potential (V *vs.* RHE)	[Oxalic acid] (M)	Working electrode	Oxalic acid conversion (%)	Faraday efficiency (%)		Yield (%)		Average current density (mA cm^{-2})	Ref.
					Glyoxylic acid	Glycolic acid	Glyoxylic acid	Glycolic acid		
1	−0.8	0.1	TNT	—	45	38	—	—	−7.0	13
2	−0.9	0.1	TNF	—	17	38	—	—	−9.0	13
3	−1.0	0.1	TNP	—	20	22	—	—	−6.0	13
4	−0.9	0.03	TiNT-60	6.8	51.1	43.8	4.7	2.1	−1.4	8
5	−1.0	0.03	TiNT-HS	25.5	25.0	61.0	11.3	14.2	−2.6	8
6	−0.8	0.03	TiO_2/Ti-M	23.0	—	50	—	—	—	20
7	−0.6	0.16	PTS-500	—	49	51	16	8	—	22
8	−0.8	0.03	TiO_2-NTF	—	26	15	—	—	−4.0	21
9	−1.0	0.03	g-C_3N_4/TiO_2-NTF	—	12	76	—	—	−4.5	21
10	−0.6	0.03	Ti/native oxides	38.4	43.0	32.8	27.3	10.5	−5.1	This work

Key: TNT = TiO_2 nanotubes, TNF = TiO_2 nano-flakes, TNP = TiO_2 nano-powders, TiNT-60 = titanium oxide nanotubes, prepared by anodic oxidation with an ageing time of 60 minutes, TiNT-HS = hydrothermally-synthesised titanium oxide nanotubes, TiO_2/Ti-M = titanium oxide-titanium mesh electrode, PTS-500 = porous titanium oxide spheres calcined at 500 °C, TiO_2-NTF = titanium oxide nanotubes ordered in thin films, g-C_3N_4/TiO_2-NTF = titanium oxide nanotubes ordered in thin films mixed with graphitic carbon nitride.

Titanium electrodes coated with native oxides have been found useful in a number of electrochemical organic syntheses.[19] However, despite several studies on the electrochemical reduction of oxalic acid using different carefully synthesised titanium oxides as catalysts,[8,13,20–22] all reports to date have suffered from low oxalic acid conversion and poor glyoxylic acid and glycolic acid yields.

Herein, we examined the catalytic effect of the native oxides of titanium in oxalic acid reduction at different applied potentials. The optimal performance was recorded at an applied potential of −0.6 V *vs.* RHE. Table 1 presents this headline result, together with some previous results from the literature on oxalic acid reduction on different forms of titanium electrodes under similar conditions and experimental durations. It is noteworthy that we have, in this work, recorded the best performance in terms of oxalic acid conversion, cumulative isolated yield of glyoxylic and glycolic acids, and selectivity towards glyoxylic acid (entry 10 in Table 1) on a Ti-based electrode in a three-electrode configuration reported to date.

The electrochemical reduction of oxalic acid was conducted in the H-cell set-up depicted in Fig. S1 in the ESI.† Chronoamperometric experiments were performed for 2 hours at each applied potential. At the end of every experiment, the liquid products from the cathodic compartment were sampled and analysed by high-performance liquid chromatography (HPLC). A chromatogram showing the reduction of oxalic acid to glyoxylic and glycolic acids is presented in Fig. S2 in the ESI.† The resulting current densities, faradaic efficiencies, oxalic acid conversion and percentage yields of the products obtained at different potentials are presented in Table S1 in the ESI.† From Fig. 2(a), it can be seen that the current densities generally increase with increasingly negative potential. However, the optimal performance of the titanium electrode (Ti/Ti_xO_y) in terms of oxalic acid conversion and product yield were found at −0.6 V *vs.* RHE. The re-usability of the electrode was probed by employing the same electrode in three successive bulk electrolysis experiments at −0.6 V *vs.* RHE, as shown in Fig. S3 (ESI†). The current densities and the corresponding product yields show only modest differences, suggesting that the electrode can be re-used without significantly altering its behaviour. The performance of the electrode was tested over a longer duration of 12 h at applied potentials of −0.6 V (Fig. S4, ESI†) and −0.5 V *vs.* RHE (Fig. S5, ESI†). In both cases, similar behaviour was observed; namely, glyoxylic acid is the primary product in the first hours of the reaction, but as the duration extends (and as glyoxylic acid undergoes further reduction), glycolic acid becomes the dominant product.[23–25] Operating at −0.5 V *vs.* RHE reduces conversions and yields a small amount but does not fundamentally alter the reaction profile or the selectivity for either product to a significant degree.

At potentials more negative than −0.6 *vs.* RHE, the faradaic efficiency tends to drop, as depicted in Fig. 2(b). This is most likely because of competitive hydrogen evolution or further conversion of the products to by-products. This at least partly accounts for why the faradaic efficiencies are generally less than 100%.[26] At −0.6 *vs.* RHE, the conversion of oxalic acid was 38.4% ± 1.85, and the cumulative faradaic efficiency was 75.8%, corresponding to 43.0% ± 2.78 and 32.8% ± 2.46 for glyoxylic and glycolic acid production, respectively (Table 1, entry 10).

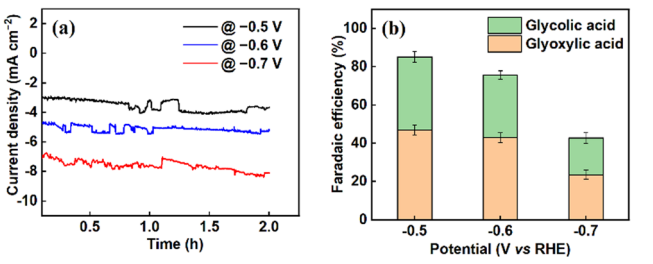

Fig. 2 (a) The current densities of titanium electrodes at three different applied potentials (−0.5 V, −0.6 V and −0.7 V *vs.* RHE) and (b) the average faradaic efficiency for production of glyoxylic and glycolic acids during bulk electrolysis of 0.03 M oxalic acid for 2 hours, using Ti foil as a working electrode and Pt foil as a counter electrode in an H-cell at 25 °C.

This conversion is slightly higher than that reported by Abramo *et al.*,[8] which gives the highest previously reported value (of 25.5%) for oxalic acid conversion on modified titanium electrodes, albeit at a more negative applied potential (Table 1, entry 5).

To properly understand the stability of (and any potential changes in) the native oxides of titanium, the electrodes were subjected to various analyses before and after electrolysis. Firstly, cyclic voltammetry was obtained on an electrode before and after 12 h of bulk electrolysis at −0.6 V *vs.* RHE. This revealed only modest changes in the voltammogram's profile compared to the pre-electrolysis state, as depicted in Fig. S6 (ESI†).

Additional analysis was then performed using X-ray diffraction (XRD), X-ray photoelectron spectroscopy (XPS), ellipsometry, atomic force microscopy (AFM), electrochemically active surface area (ECSA) determination, and electrochemical impedance spectroscopy (EIS). The XRD patterns in Fig. S7 of the ESI† exhibit multiple distinct peaks associated with pure titanium and its naturally occurring oxides (Ti/Ti_xO_y), alongside titanium's anatase or rutile crystalline structures.[27,28] However, additional diffraction peaks with relatively low intensities were also observed, corresponding to oxygen-deficient forms of Ti_xO_y-type species.[29] These peaks are indicative of shear planes in the crystal structure and are commonly referred to as suboxides.[30,31] A confirmatory check was made by matching and extracting the spectral data from the XRD database of titanium (JCPDS: 1512547) confirming the presence of TiO_2 (JCPDS: 9004144), Ti_2O (JCPDS: 1532773), Ti_3O_5 (ICSD: 98-001-5894),[32] and Ti_4O_7 (ICSD: 98-001-9017),[27,33] which are electrically conductive Ti oxides.[32]

Similarly, XPS was employed to detect the composition of the titanium oxides on the electrodes. The high-resolution spectroscopy results of Ti^{4+} are shown in Fig. 3(a and b). After deconvolution, there are two main peaks into which all other peaks were resolved (at the binding energy levels of 454.5 eV and 458.4 eV), representing Ti^{4+} $2P_{3/2}$ and Ti^{4+} $2P_{1/2}$, respectively.[26] Fig. 3(c and d) illustrates that the O 1s core level spectrum exhibits main peaks at 530.1 eV for O^{2-}, 532.0 eV for Ti–OH, and 533.0 eV for Ti–H_2O,[34] showcasing slight variations in these binding energies among different metal oxides. These peaks are ascribed to metallic oxides (Ti–O bonds)[35,36] and are consistent with the binding energy of O_2^- in the TiO_2 lattice.[34,37] Fig. S8 of the ESI† presents the full XPS spectrum of the titanium electrode. A peak at about 580 eV (assigned to Ti 2s) in the spectrum grows after electrolysis. Both the Ti 2p and Ti 2s peaks originate from Ti metal.[38] This observation is consistent with the idea that the titanium oxide layer becomes thinner during electrolysis (allowing underlying Ti metal to be more clearly detected) and agrees with the ellipsometry results, which also suggest a decrease in the thickness of the oxides.

Ellipsometry measurements of the electrode showed a decrease in the thickness of the native oxides from 48.4 ± 0.4 nm before electrolysis to 17.9 ± 1.5 nm after electrolysis, as depicted in Table S2 (ESI†). The reduction in the thickness of the native oxides of titanium after electrolysis could be due to the etching of the oxides by the acid,[39,40] or else to the reduction of part of the oxide to the metal during electrolysis. The electrode's ellipsometry fitting model is represented in Fig. S9 of the ESI.† Atomic force microscopy (AFM) analysis was performed to determine the roughness and morphology of the surface of the electrode before and after electrolysis. The root mean square roughness of the electrode (R_q) increased from 35.2 nm before electrolysis to 49.7 nm after electrolysis, as shown in Table S3 of the ESI.† This would be consistent with mass transfer and diffusion processes occurring on the surface of the electrode during electrolysis. AFM 3D-topography images of the surface of the electrode before and after the electrolysis are presented in Fig. 4.

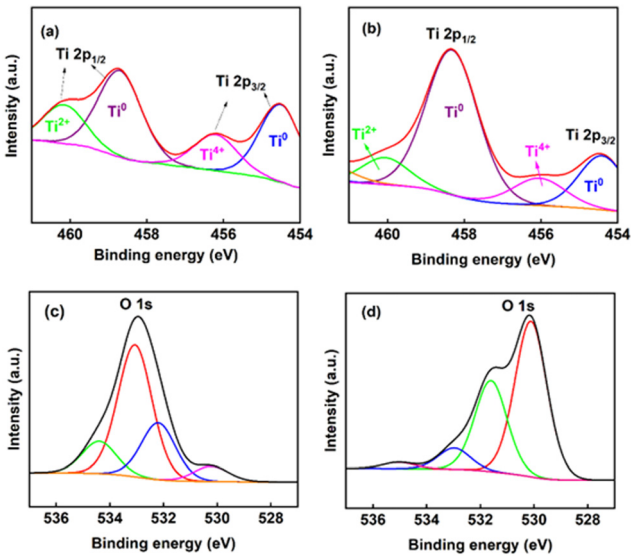

Fig. 3 Deconvoluted XPS spectra of the titanium electrode (a) Ti 2p spectra before electrolysis, (b) Ti 2p spectra after electrolysis, (c) O 1s spectra before electrolysis, and (d) O 1s spectra after electrolysis.

The electrode's electrochemically active surface area (ECSA) was determined by cyclic voltammetry at different scan rates ranging from 10 mV s^{-1} to 1000 mV s^{-1} (see Fig. S10 of the ESI†). Thereafter, the double-layer capacitance (C_{DL}) and specific capacitance (C_S) of the electrode were evaluated using eqn (S6) and (S7) in the ESI,† respectively. Subsequently, the ECSA value was computed using eqn (S5) (ESI†), and the value of 1.49 cm^{-2} was obtained.

Electrochemical impedance spectroscopy (EIS) of the electrode was employed to analyse the interfacial behaviour and to determine the electrochemical parameters on the electrode surface,[41] under optimal conditions during electrolysis at −0.6 V *vs.* RHE. Fig. S11 of ESI† shows the electrochemical

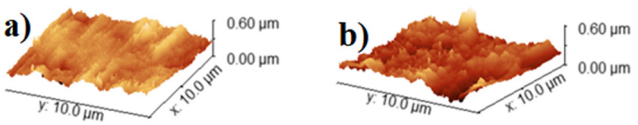

Fig. 4 AFM analysis of titanium electrode surfaces (a) before and (b) after electrolysis.

responses of the titanium electrode before and after electrolysis. The electrode exhibits smaller semicircles after electrolysis compared to the pre-electrolysis state. This decrease suggests better conductance of the electrodes after electrolysis. This phenomenon is consistent with some of the oxide layers being removed, perhaps by *in situ* reduction at the applied cathodic potentials, which is in agreement with the XPS and ellipsometry data. The equivalent circuit model and the electrical parameters of the proposed equivalent circuits obtained after fitting the EIS data are presented in Fig. S12 and Table S4 of the ESI.†

In conclusion, this work presents the first evaluation of the catalytic effect of the native oxides of titanium (Ti/Ti_xO_y) in the electrochemical reduction of oxalic acid. This native oxide-coated electrode showed superior performance in terms of oxalic acid conversion and cumulative (glyoxylic + glycolic) product yield compared to other (deliberately) modified titanium-based electrodes in a three-electrode system. The surface morphology, oxide thickness, physical and electrochemical stability of the native oxides were examined using XRD, XPS, EIS, AFM, and ellipsometry. Despite minor changes and the reduced oxide thickness observed after electrolysis, the native oxide-coated electrode produced glyoxylic and glycolic acids in good yield compared to previously reported Ti-based systems. These results, in turn, suggest that unmodified Ti electrodes bearing the naturally forming native Ti-oxides on their surface are competent for oxalic acid reduction and that deliberate modifications to the Ti surface may be unnecessary for acceptable performance.

This work was supported by the EPSRC (EP/W033135/1 and EP/W02134X/1). HS thanks his sponsor (the Petroleum Technology Development Fund, Nigeria) for funding his studies (PTDF/ED/OSS/PHD/HA/1638/19). MDS thanks the Royal Society for a University Research Fellowship (URF\R\211007).

Data Availability: The data underpinning this study have been deposited in the University of Glasgow's Enlighten database under accession code **https://doi.org/10.5525/gla.researchdata.1648**.

Conflicts of interest

There are no conflicts to declare.

Notes and references

1 V. Boor, J. E. B. M. Frijns, E. Perez-Gallent, E. Giling, A. T. Laitinen, E. L. V. Goetheer, L. J. P. Van Den Broeke, R. Kortlever, W. De Jong, O. A. Moultos, T. J. H. Vlugt and M. Ramdin, *Ind. Eng. Chem. Res.*, 2022, **61**, 14837–14846.
2 H. Sale, G. R. Ubbara and M. D. Symes, *Sustainable Energy Fuels*, 2023, 5093–5100.
3 M. A. Farkhondehfal, U. Savino, A. Chiodoni, C. F. Pirri and A. Sacco, *Electrocatalysis*, 2023, **14**, 195–201.
4 S. Im, S. Saad and Y. Park, *Electrochem. Commun.*, 2022, **135**, 107204.
5 R. Paul, Q. Zhai, A. K. Roy and L. Dai, *Interdiscip. Mater.*, 2022, **1**, 28–50.
6 Y. Lu, X. L. Liu, L. He, Y. X. Zhang, Z. Y. Hu, G. Tian, X. Cheng, S. M. Wu, Y. Z. Li, X. H. Yang, L. Y. Wang, J. W. Liu, C. Janiak, G. G. Chang, W. H. Li, G. Van Tendeloo, X. Y. Yang and B. L. Su, *Nano Lett.*, 2020, **20**, 3122–3129.
7 S. Perathoner and G. Centi, *Catal. Today*, 2019, **330**, 157–170.
8 F. P. Abramo, F. De Luca, R. Passalacqua, G. Centi, G. Giorgianni, S. Perathoner and S. Abate, *J. Energy Chem.*, 2022, **68**, 669–678.
9 Y. L. Niu and L. J. Zhai, *Monatsh. Chem.*, 2014, **145**, 201–207.
10 Q. Shan Wang, Y. Chao Yuan, C. Fan Li, Z. Rui Zhang, C. Xia, W. Guo Pan and R. Tang Guo, *Small*, 2003, 1–25.
11 M. Valderrama, R. van Putten and G. M. Gruter, *Eur. Polym. J.*, 2019, **119**, 445–468.
12 F. Zhao, F. Yan, Y. Qian, Y. Xu and C. Ma, *J. Electroanal. Chem.*, 2013, **698**, 31–38.
13 M. A. Farkhondehfal, U. Savino, A. Chiodoni, C. F. Pirri and A. Sacco, *Electrocatalysis*, 2023, **14**, 195–201.
14 L. Wang, H. Yu, S. Wang, L. Qiao and D. Sun, *Appl. Surf. Sci.*, 2019, **496**, 143657.
15 S. Guo, Z. Xu, W. Hu, D. Yang, X. Wang, H. Xu, X. Xu, Z. Long and W. Yan, *Catalysis*, 2022, **12**, 618.
16 Y. Su, Z. Wang, A. Legrand, T. Aoyama, N. Ma, W. Wang, K. I. Otake, K. Urayama, S. Horike, S. Kitagawa, S. Furukawa and C. Gu, *J. Am. Chem. Soc.*, 2022, **144**, 6861–6870.
17 B. Xu, H. Y. Sohn, Y. Mohassab and Y. Lan, *RSC Adv.*, 2016, **6**, 79706–79722.
18 S. Guan, Y. Cheng, L. Hao, H. Yoshida, C. Tarashima, T. Zhan, T. Itoi, T. Qiu and Y. Lu, *Sci. Rep.*, 2023, **13**, 1–9.
19 L. Liu, X. Gu, Z. Ji, W. Zou, C. Tang, F. Gao and L. Dong, *J. Phys. Chem. C*, 2013, **117**, 18578–18587.
20 M. Sadakiyo, S. Hata, X. Cui and M. Yamauchi, *Sci. Rep.*, 2017, **7**, 1–9.
21 F. de Luca, R. Passalacqua, F. P. Abramo, S. Perathoner, G. Centi and S. Abate, *Chem. Eng. Trans.*, 2021, **84**, 37–42.
22 R. Watanabe, M. Yamauchi, M. Sadakiyo, R. Abe and T. Takeguchi, *Energy Environ. Sci.*, 2015, **8**, 1456–1462.
23 W. Ke, C. C. Stoumpos, J. L. Logsdon, M. R. Wasielewski, Y. Yan, G. Fang and M. G. Kanatzidis, *J. Am. Chem. Soc.*, 2016, **138**, 14998–15003.
24 J. E. Carrera-Crespo, J. Ghilane, H. Randriamahazaka, S. Ammar and I. González, *J. Electrochem. Soc.*, 2017, **164**, H286–H292.
25 N. P. Shetti, D. S. Nayak, S. J. Malode and R. M. Kulkarni, *J. Electrochem. Soc.*, 2017, **164**, B3036–B3042.
26 W. Song, Y. Zhang, H. Jin, M.-R. Kim, S. Kim and I. Kim, *J. Electrochem. Soc.*, 2017, **164**, E260–E264.
27 Z. Ertekin, N. Ö. Pekmez and K. Pekmez, *J. Solid State Electrochem.*, 2020, **24**, 975–986.
28 X. Zhang, C. Wang, J. Chen, W. Zhu, A. Liao, Y. Li, J. Wang and L. Ma, *ACS Publ.*, 2014, **6**, 32.
29 Y. Su, K. Ichi Otake, J. J. Zheng, H. Xu, Q. Wang, H. Liu, F. Huang, P. Wang, S. Kitagawa and C. Gu, *Nat. Commun.*, 2024, **15**, 1–7.
30 Y. Su, K. Ichi Otake, J. J. Zheng, S. Horike, S. Kitagawa and C. Gu, *Nature*, 2022, **611**, 289–294.
31 C. Gu, N. Hosono, J. J. Zheng, Y. Sato, S. Kusaka, S. Sakaki and S. Kitagawa, *Science*, 2019, **363**, 387–391.
32 S. H. Hong, *Acta Chem. Scand.*, 1982, **36**, 207–217.
33 M. Watanabe, *Phys. Status Solidi C*, 2009, **6**, 260–263.
34 E. McCafferty and J. P. Wightman, *Appl. Surf. Sci.*, 1999, **143**, 92–100.
35 P. Gao, J. Wu, Q. J. Liu and W. F. Zhou, *Chin. Phys. B*, 2010, **19**(8), 087103.
36 Y. Su, B. Li, H. Xu, C. Lu, S. Wang, B. Chen, Z. Wang, W. Wang, K. I. Otake, S. Kitagawa, L. Huang and C. Gu, *J. Am. Chem. Soc.*, 2022, **144**, 18218–18222.
37 S. Wang, Z. Xie, D. Zhu, S. Fu, Y. Wu, H. Yu, C. Lu, P. Zhou, M. Bonn, H. I. Wang, Q. Liao, H. Xu, X. Chen and C. Gu, *Nat. Commun.*, 2023, **14**, 6891.
38 D. Jaeger and J. Patscheider, *J. Electron Spectrosc. Relat. Phenom.*, 2012, **185**, 523–534.
39 J. Winiarski, A. Niciejewska, M. Górnik, J. Jakubowski, W. Tylus and B. Szczygieł, *RSC Adv.*, 2021, **11**, 21104–21115.
40 P. Vlcak, J. Fojt, J. Drahokoupil, V. Brezina, J. Sepitka, T. Horazdovsky, J. Miksovsky, F. Cerny, M. Lebeda and M. Haubner, *Mater. Sci. Eng., C*, 2020, **115**, 111065.
41 S. Popescu, C. Ungureanu, A. M. Albu and C. Pirvu, *Prog. Org. Coat.*, 2014, **77**, 1890–1900.

